Applied Catalysis B: Environmental 218 (2017) 240–248

Contents lists available at ScienceDirect

Applied Catalysis B: Environmental

journal homepage: www.elsevier.com/locate/apcatb

Promotion effects of alkali- and alkaline earth metals on catalytic activity of mesoporous Co_3O_4 for 4-nitrophenol reduction

Batsile M. Mogudi, Phendukani Ncube, Ndzondelelo Bingwa, Naphtaly Mawila, Shitshembiso Mathebula, Reinout Meijboom*

Department of Chemistry, University of Johannesburg, PO Box 524, Auckland Park, Johannesburg 2006, South Africa

ARTICLE INFO

Article history:
Received 22 November 2016
Received in revised form 1 June 2017
Accepted 17 June 2017
Available online 19 June 2017

Keywords:
Heterogeneous catalysts
Promoter
Doped cobalt oxide
4-Nitrophenol reduction
Kinetics

ABSTRACT

Mesoporous cobalt oxides doped with alkali (Li, Na, K, Cs) and alkaline earth (Mg, Ca) metals were synthesized and evaluated for their catalytic activity in the reduction of 4-nitrophenol. The prepared materials were characterized using scanning electron microscopy (SEM), transmission electron microscopy (TEM), powder X-ray diffraction (XRD), Brunauer–Emmet–Teller (BET) and hydrogen temperature programmed reduction (H_2-TPR) analyses. The characterization techniques used showed the materials to consist of mono-dispersed nanoparticle aggregates with connected, well defined intra-particle voids and the crystalline phase of the cobalt oxide to be cubic Co_3O_4, while the pore diameters ranged from 12.1 to 19.2 nm depending on the metal ion dopant. The reduction of 4-nitrophenol was chosen as a well-controlled model reaction allowing us to determine the catalytic activity as a function of alkali or alkaline earth dopant. Calcium doped cobalt oxide was found to be the most catalytically active with an apparent rate constant of 3.76×10^{-3} s^{-1} and the order with respect to dopant was Ca > Cs > Mg > Li > K > Na. From characterization of the catalysts by SEM, TEM and H_2-TPR promotion effects of the dopants were found to be due to electronic changes in the catalysts as a result of doping rather than structural changes. The kinetics of the most active calcium doped catalyst was modeled in terms of Langmuir–Hinshelwood kinetics. The Langmuir–Hinshelwood surface rate constant for Ca-doped Co_3O_4 was 5.47×10^{-5} mol m^{-2} s^{-1} compared to the undoped Co_3O_4 at 5.33×10^{-6} mol m^{-2} s^{-1}. Activation energies were calculated to be 51.3 kJ mol^{-1} and 50.7 kJ mol^{-1} for undoped and Ca-doped Co_3O_4.

1. Introduction

Mesoporous metal oxides (MMOs) [1,2] have received immense attention in catalysis due to them having multiple oxidation states as compared to the conventional mesoporous silica and aluminosilicates [3–6]. Mesoporous cobalt oxides are extensively used in a wide range of catalytic applications as cobalt is both relatively less expensive compared to noble metals and offers catalytic activity comparable to the noble metals [7,8]. In order to improve the catalytic properties of the MMOs, dopants and promoters are often incorporated into the materials [9–12].

Alkali and alkaline earth promoted cobalt oxides have been reported to have improved catalytic activity towards various reactions including the decomposition of NO_x species [13–16] and various redox reactions [9,17,18]. The mechanism of alkali and alkaline earth promotion has been proposed to be due to the metal dopants being structural [19] or electronic promoters [13,20–22] in the various catalytic properties. In their research on N_2O decomposition using alkali and alkaline earth doped catalysts, Xue et al. [13] found that the catalytic activity was greatly increased and that the promotion effect was in the order Li < Na < K < Rb < Cs < Mg < Ca < Sr, Ba. The promotion effect of alkali and alkaline earth metals on the catalytic reduction of 4-nitrophenol using mesoporous cobalt oxide was investigated in this study. Nitro-aromatic compounds are toxic organic species which are produced as by-products in the pharmaceutical, agrochemical, urethane, textile and dye chemical industries [23,24]. There is always, therefore, a need to develop economic and green catalysts for the remediation of sources contaminated with these toxic organic compounds by reducing them to the less toxic amines. Precious metals such as gold, palladium, platinum and ruthenium have been used extensively as catalysts [25–28] for this reduction. Since precious metals are expensive, there is a need to replace them with non-precious metals such as cobalt.

* Corresponding author.
E-mail addresses: rmeijboom@uj.ac.za, reinout.meijboom@gmail.com (R. Meijboom).

http://dx.doi.org/10.1016/j.apcatb.2017.06.045
0926-3373/

Mesoporous cobalt oxides were catalytically active in the reduction of 4-nitrophenol, with the activity dependent on the morphology of the catalysts [29]. Literature reports by Sahiner et al. [24] and by Mandlimath et al. [30] have also shown that cobalt oxides are catalytically active in the reduction of 4-nitrophenol. In this work doping cobalt oxide with alkali and alkaline earth metals enhances the catalytic activity in the 4-nitrophenol reduction when compared to the undoped cobalt oxide. Furthermore, the catalytic activity of the calcium-doped catalysts on the reduction of 4-nitrophenol by borohydride in aqueous solution, proceeds via a Langmuir–Hinshelwood (L–H) model [31–33]. We present a full kinetic analysis of the heterogeneous-catalyzed reduction of 4-nitrophenol with sodium borohydride using calcium doped mesoporous cobalt oxide catalysts. There is no reported detailed kinetic analysis of the reduction of 4-nitrophenol using alkali and alkaline earth doped mesoporous cobalt oxide catalysts.

2. Experimental

2.1. Materials

All chemicals used were reagent-grade and used as received. Cobalt(II) nitrate hexahydrate (≥98%) [$Co(NO_3)_2{\cdot}6H_2O$], 1-butanol, poly(ethylene glycol)-*block*-poly(propylene glycol)-*block*-poly(ethylene glycol) (PEO20-PPO70-PEO20 or Pluronic P123, av. M_n = 5800), sodium borohydride ($NaBH_4$, ≥96.0%), 4-nitrophenol (≥99.5%), $LiNO_3$ (≥99.0%), $NaNO_3$ (≥99.0%), KNO_3 (≥99.0%), $Mg(NO_3)_2{\cdot}6H_2O$ (≥99.0%) and $Ca(NO_3)_2{\cdot}4H_2O$ (≥99.0%) were all purchased from Sigma-Aldrich. Concentrated nitric acid (68–70% HNO_3) was purchased from Rochelle Chemicals (RSA).

2.2. Synthesis of alkali- and alkaline earth-doped mesoporous cobalt oxides

To synthesize alkali- and alkaline earth-doped mesoporous cobalt oxides a method adapted from the literature was used [34]. In short, $Co(NO_3)_2{\cdot}6H_2O$ (10 g, 0.035 mol) was dissolved in a solution containing P123 (5.0 g, 8.62×10^{-4} mol) and HNO_3 (4.8 g, 0.076 mol) in 1-butanol (34 g, 0.66 mol). An appropriate amount of XNO_3 (X = Li, Na, K) or $X(NO_3)_2$ (X = Mg, Ca) was added to give 2% (mol/mol) of each dopant. The red solution was stirred and then placed in an oven at 50 °C for 12 h to remove the solvent. The formed gel was then placed in an oven at 120 °C for 3.5 h. The obtained powder was washed with ethanol several times, and dried in a vacuum oven. The resulting red powder was calcined at 150 °C for 12 h with a heating rate of 1 °C/min. All heating cycles were performed in air.

2.3. Characterization

Powder X-ray diffraction analyses were performed on a Rigaku Miniflex-600 diffractometer with Cu Kα radiation (λ = 1.5406 Å) at room temperature. Both low angle (2θ = 0.5–8°) and wide angle (2θ = 10–90°) diffraction patterns were measured. Nitrogen sorption measurements were performed on a Micromeritics Tristar 3000 sorption system. The samples were degassed at 90 °C for 18 h prior to the experiments. The surface areas were calculated by the Brunauer-Emmett-Teller (BET) method, and the pore size distributions were obtained by the Barrett–Joyner–Haleda (BJH) method from the desorption branch of the isotherms. Scanning Electron Microscopy (SEM) images were taken on a Tescan Vega 3LMH scanning electron microscope with the samples carbon-coated on copper grids using an Agar Turbo Carbon Coater. High resolution transmission electron microscopy (HRTEM) was performed on a JEOL JEM-2100F electron microscope with an accelerating voltage of 200 kV. Temperature programmed analyses were conducted on a Micromeritics Autochem II. About 30 mg of material was packed in a quartz tube reactor. The loaded samples were pretreated in an inert gas flow (Ar) at 200 °C for 1 h to clean the catalyst surface before each test. In H_2-TPR measurements, 10% H_2/Ar was passed through the catalyst bed at a flow rate of 50 ml min^{-1} while the temperature was ramped from 30 °C to 500 °C with a heating ramp rate of 10 °C min^{-1}. XPS data were acquired at room temperature with a SPECS Phoibos 150 electron energy analyser, using a monochromated Al Kα photon source ($h\nu$ = 1486.71 eV). The overall energy resolution was set to 0.5 eV for all the spectra. The binding energy was calibrated with respect to the main peak in the C 1*s* core level (284.6 eV). To counteract the effect of surface charging, samples were irradiated with a low energy electron flood gun during measurements (electron energy: 3 eV).

2.4. Catalytic activity

The kinetic evaluation was performed by detecting the extinction of 4-nitrophenol (4-NP) via UV–vis spectrophotometry using a Shimadzu UV1800 equipped with a CPS-240A Cell Positioner and CPS-Controller for temperature regulation. Stock solutions of 4-NP (1000 μM) and $NaBH_4$ (1.0 M) were first prepared. Initial spectrophotometric scans were performed using the full spectrum range of λ 200–800 nm with readings taken every three minutes, in quartz cuvettes. Subsequently all kinetic measurements were performed in disposable polystyrene cuvettes. In a typical run, the appropriate amount of 4-NP and catalysts was mixed in a 50 ml jacketed flask and the volume made to 25 ml with deionized water. The mixture was then degassed by bubbling with nitrogen for 30 mins. The jacketed flask was then connected to a pre-heated water bath at the desired temperature. Then a 100 fold excess of $NaBH_4$ was added to start the reaction and aliquots of 3 ml were taken at 3 min intervals, filtered and the UV–vis spectrum taken. For the kinetic runs to obtain L–H parameters, two sets of experiments were performed at 25 °C with a constant catalyst amount. The first data set was obtained for a constant $NaBH_4$ concentration while varying the concentration of 4-NP. The second set, k_{app} values were obtained for a run were the concentration of $NaBH_4$ was varied while keeping 4-NP concentration constant. For thermodynamic analysis, the temperature of the water bath was varied from 20 to 35 °C. From the raw experimental data, k_{app} values were determined using the Kinetic Studio software [35] while the L–H fitting of the data was performed using the Origin Pro 8.5 graphing and modeling software [36].

3. Results and discussion

3.1. Synthesis and characterization of mesoporous doped Co_3O_4 catalysts

Mesoporous cobalt oxides doped with alkali (Li, Na, K and Cs) and with alkaline earth (Mg and Ca) metals were synthesized using a method reported in the literature [37]. Powder X-ray diffraction (*p*-XRD) patterns are shown in Fig. 1 (a) for the undoped as well as alkali and alkaline earth metal ion-doped mesoporous cobalt oxide materials. From the *p*-XRD analysis with the Match™ Software, all the materials showed a typical spinel Co_3O_4 pattern (JCPDS 090418) with a cubic crystal system. Crystallite sizes of the materials estimated from *p*-XRD analysis showed an insignificant change upon doping with all the metals, an observation that could be explained by the fact that only a small amount of dopant (2%) was added. From N_2 sorption analysis all doped materials maintained the characteristic Type IV adsorption isotherms, with a Type I hysteresis loop typical of a regular ordered mesoporous structure (Fig. 1b). Doping of the cobalt oxide with the different metal ions resulted in a decrease in the surface area of the materials as summarized

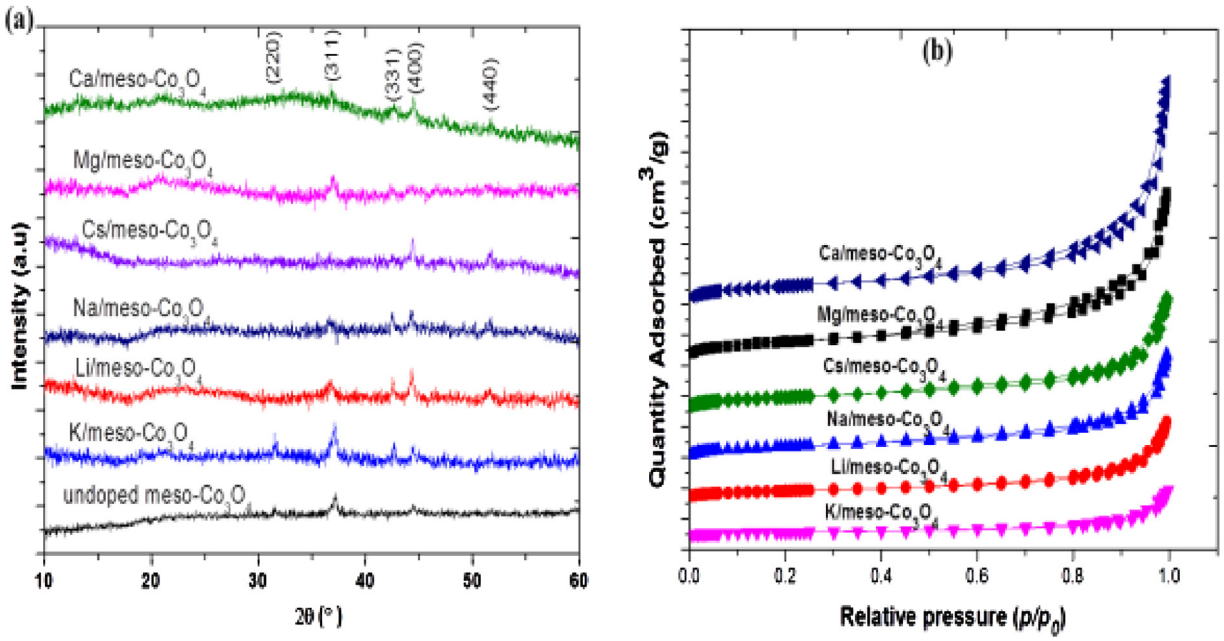

Fig. 1. Characterization of prepared materials: (a) *p*-XRD patterns (b) N_2 sorption isotherms of undoped and doped mesoporous cobalt oxides.

Table 1
BET surface areas, BJH pore sizes and pore volumes as well as crystallite sizes[a] of the prepared doped and undoped mesoporous cobalt oxide catalysts.

Catalyst	BET surface area (m^2/g)	BJH pore size diameter (nm)	Pore volume (cm^3)	Crystallite size[a] (nm)	% dopant[b]
Undoped *meso*-Co_3O_4	32.9	12.1	0.093	14.9	–
Li/Meso-Co_3O_4	10.7	15.0	0.039	14.3	2 ± 1.09
Na/Meso- Co_3O_4	17.3	12.9	0.053	14.8	2 ± 0.74
K/Meso- Co_3O_4	4.70	17.0	0.022	14.9	2 ± 0.32
Cs/Meso- Co_3O_4	17.0	12.8	0.058	15.0	2 ± 0.20
Mg/Meso- Co_3O_4	22.1	13.6	0.085	15.1	3 ± 0.41
Ca/Meso- Co_3O_4	20.9	19.2	0.11	15.1	2 ± 0.12

[a] Crystallite sizes calculated from *p*-XRD using the Scherer equation.
[b] % dopant determined by ICP-OES.

in Table 1, in which we also tabulate pore sizes, pore volumes and crystallite sizes of the catalysts. The trend observed was that doping with Group II metal, Mg (22.1 m^2/g) and Ca (20.9 m^2/g), decreased the surface area to a lesser extent when compared to Group I metal, Li (10.7 m^2/g), Na (17.3 m^2/g), K (4.7 m^2/g) and Cs (17.0 m^2/g). A similar decrease in surface area for mesoporous cobalt oxides doped with alkali and alkaline earth metal ions was observed in the work by Song et al. [38] as well as by Poyraz et al. [37]. Microscopic analysis of the doped cobalt oxide materials by SEM (Fig. 2a and d) and by TEM (Fig. 2b and e) further confirmed the mesoporosity of the materials. The morphology of the doped Co_3O_4 catalyst materials did not differ significantly from the undoped Co_3O_4, for the same amount (~2%) of each different dopant, again indicating no structural change upon doping. However, when the amount of the Ca dopant was increased from 1.1% to 7.0% some morphological changes were observed. This could be explained by the fact that increasing tha amount of dopant completely blocks the pores of the mesoporous cobalt oxide structure. This pore blockage with increasing Ca dopant was observed and is shown in the SEM images in the Supplementary Information (Fig. S3). The presence of each dopant in the catalyst materials was confirmed by EDX analysis (Fig. 2c and d). Representative SEM and TEM images as well as EDX spectra for Ca/Co_3O_4 and K/Co_3O_4 are shown in Fig. 2, while the rest of SEM (Fig. S1), TEM (Fig. S2) and EDX (Fig. S3) results for the other catalysts are presented in the Electronic Supplementary information.

Since no structural change was observed (from SEM and TEM analyses) upon doping with the same amount of different dopant, we performed temperature programmed reduction using hydrogen (H_2-TPR) to investigate the effect of doping on redox properties of cobalt oxide catalysts to see if doping resulted in any electronic changes in our catalysts. H_2-TPR profiles (Fig. 3a) show that the reduction of the doped Co_3O_4 catalysts, like that of the undoped Co_3O_4, occurs in two steps. The first peak appearing in the range 200–300 °C corresponds to the reduction from Co^{3+} to Co^{2+} and the broader peak in the range 300–400 °C can be ascribed to the reduction of Co^{2+} to metallic cobalt as previously reported in the literature [39–42]. From the H_2-TPR profiles in Fig. 3a we determined the total peak areas using the Origin© software [36]. From the peak areas we calculated the H_2 consumption by assuming that the reduction of Co in Co_3O_4 would result in H_2: Co ration of 1.33 [43]. So from the peak area of the undoped Co_3O_4 as a reference, we calculated relative H_2: Co ratios of the doped catalysts and the values are shown in Fig. S2 (Supplementary information). The order of the calculated ratios for the different dopants was Ca < Cs < Mg < Li < K < Na showing that the least amount of H_2 was consummed for the reduction of Ca/Co_3O_4 catalyst. The same order was observed in the catalytic activity of the doped catalysts (Section 3.2) indicating that doping with alkali and alkaline earth metals made the doped Co_3O_4 better catalysts in the reduction of 4-NP.

From the characterization by SEM, TEM and H_2-TPR analyses we concluded that the observed improved catalytic activity was due to electronic effects rather than structural changes resulting

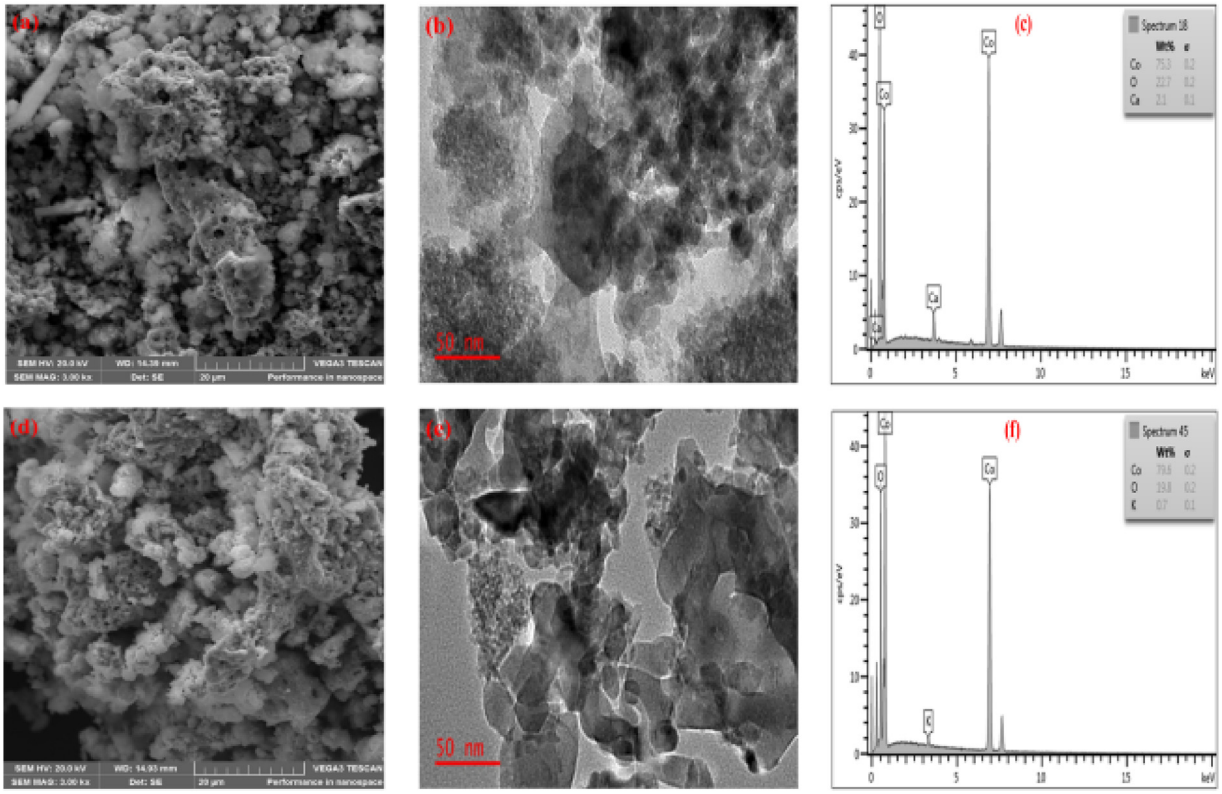

Fig. 2. Representative SEM and TEM images as well as EDX spectra of (a, b, c) Ca/Co_3O_4 and (d, e, f) K/Co_3O_4 catalysts.

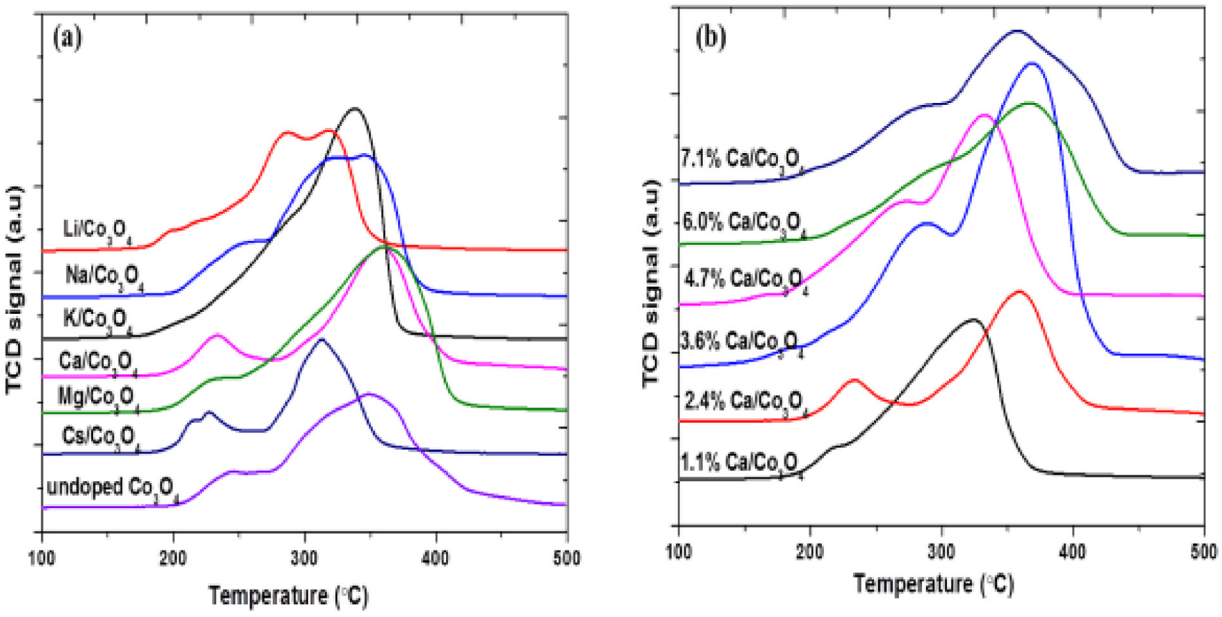

Fig. 3. (a) H_2-TPR profiles of cobalt oxides doped with different alkali and alkali earth metals and undoped Co_3O_4 and (b) H_2-TPR profiles of cobalt oxide doped to different amounts of Ca. (measurement conditions: temperature from 30 °C to 500 °C at a rate of 10 °C/min using a stream of 10% H_2/Ar balance with a flow rate of 50.11 cm^3 STP/min).

from doping. Even though there was a decrease in surface area upon doping, the dopants improved the electronic structure of the Co_3O_4 catalysts making them better reducing agents in the 4-NP reduction with borohydride. Such electronic promotion effects were explained in the literature [13] for Co-based catalysts to be due to the fact that promoters facilitate the electron donation process from Co^{2+} to 4-NP and at the same time improve the reducibility of Co^{3+} to Co^{2+} which is important for the desorption of the product – 4-aminophenol – from the catalyst surface, thus enhancing the catalytic activity of the doped Co catalyst.

Preliminary XPS results were not conclusive. The effect of metal doping on the cobalt oxide did not show any obvious trends on the prominent Co $2p_{1/2}$ and $2p_{3/2}$ peaks observed for the pure Co_3O_4. Similar results have been reported in literature for a Mn system [9]. Thus, changes in catalytic activity will be discussed based on the results of other techniques.

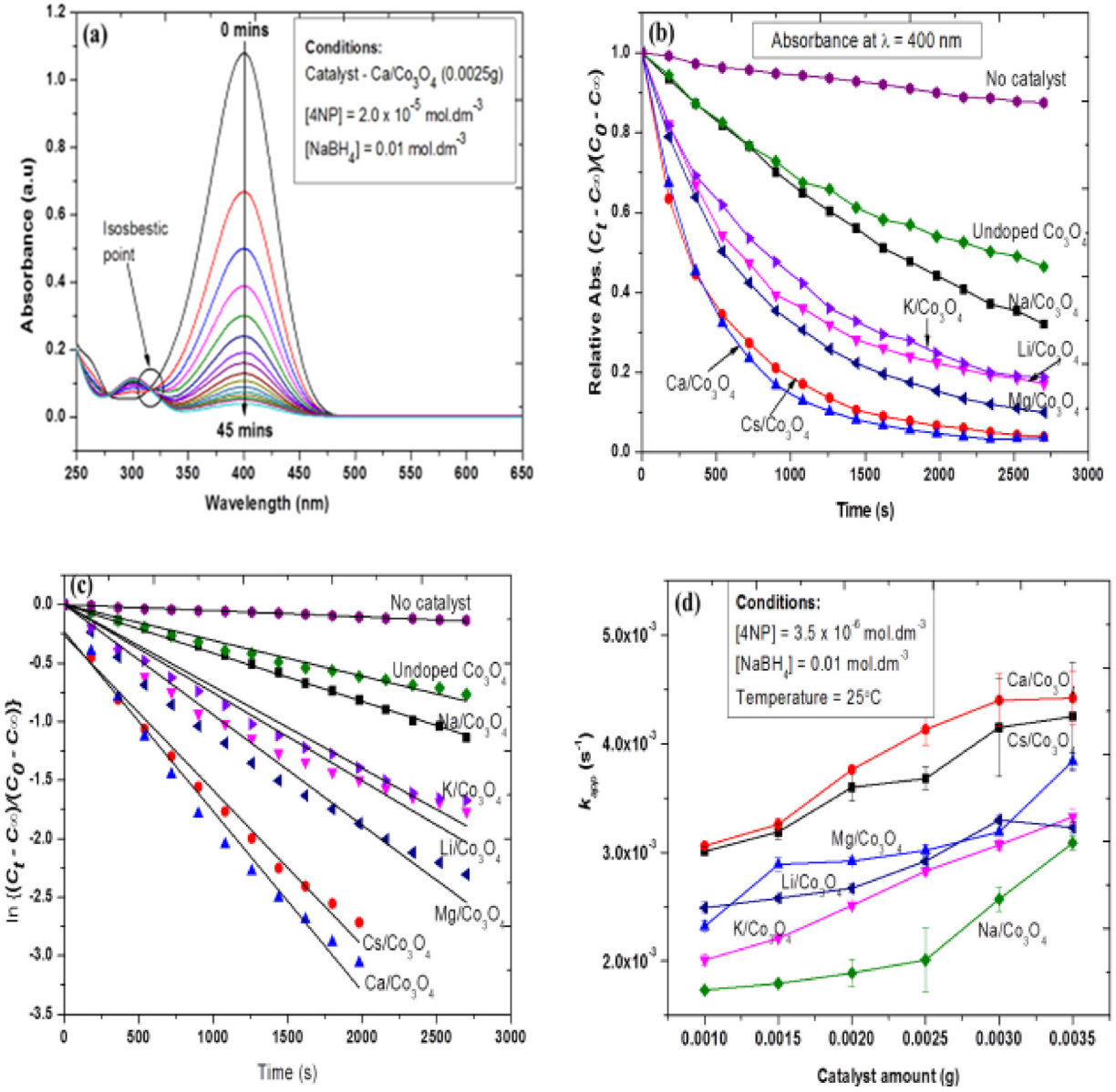

Fig. 4. (a) Typical time-resolved UV–vis spectrum of the catalyzed reduction of 4-NP over Ca-doped mesoporous Co_3O_4 catalysts. (b) Kinetic traces (at λ 400 nm) of the reduction of 4-NP over the different doped mesoporous Co_3O_4 catalysts (c) first order kinetics and (d) effect of varying catalyst loading.

3.2. Catalytic activity of catalysts and kinetic analysis of data

3.2.1. Effect of type of dopant on catalytic activity

The catalytic reduction of 4-nitrophenol (4-NP) in the presence of excess $NaBH_4$ was chosen as a model reaction to investigate the catalytic activity of the doped Co_3O_4 catalysts. This reaction can easily be monitored using UV–vis spectrophotometry by following the decrease in absorbance wavelength of maximum absorption for 4-NP at λ_{max} = 400 nm. A UV–vis profile showing this decrease for a typical catalyzed reaction using Ca/Co_3O_4 catalyst is shown in Fig. 4(a). The decrease at λ_{max} = 400 nm occurs with a simultaneously increase in absorption at λ_{max} = 300 nm corresponding to the formation of the product, 4-aminophenol. The presence of an isosbestic point in Fig. 4(a) shows that a single product is formed and therefore makes kinetic analysis of results in terms of initial rates applicable. Kinetic traces of the reduction of 4-NP over the doped and undoped mesoporous Co_3O_4 catalysts as monitored by the decrease in absorbance at λ_{max} = 400 nm are shown in Fig. 4(b). In the presence of doped Co_3O_4 catalysts there was a decrease in absorbance in the order of dopant as follows Ca > Cs > Mg > Li > K > Na. An insignificant decrease in absorbance was observed when no catalyst was used, while all doped catalysts showed enhanced activity when compared to the undoped Co_3O_4.

A plot of the experimental data according to Eq. (1) for the different catalysts gave a linear relationship (Fig. 4c) showing that the reaction follows first-order kinetics with respect to 4-NP. In Eq. (1), C_0 and C_t denote the concentrations of 4-NP at initial time and at time t, respectively, C_∞ is the final concentration of 4-NP, while k_{app} represents the apparent (or observed) rate constant.

$$ln\left(\frac{C_t - C_\infty}{C_0 - C_\infty}\right) = k_{app} \cdot t \quad (1)$$

The observed first-order kinetics with respect to 4-NP suggests that the reduction of 4-NP on our doped Co catalysts proceeds via a non-dissociative (unimolecular) adsorption of 4-NP on the catalyst surface, consistent with Langmuir–Hinshelwood mechanism proposed later in Section 3.2.3. The L–H mechanism proposes that

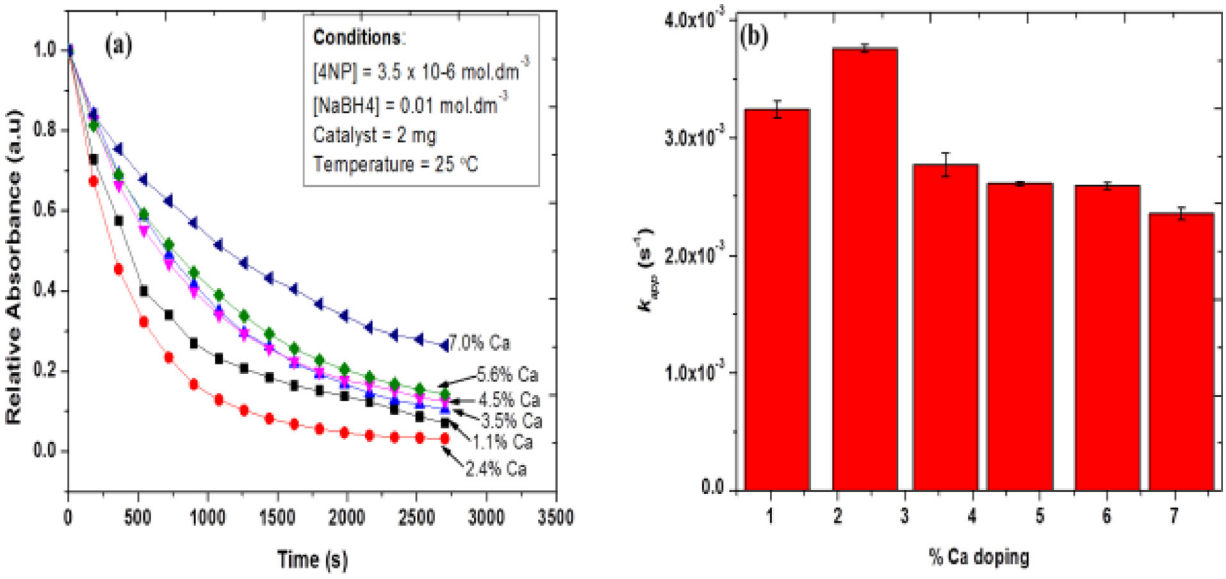

Fig. 5. Kinetic traces (at λ 400 nm) of the reduction of 4-NP over the different% Ca-doped mesoporous Co_3O_4 catalysts. Conditions—catalyst amount = 0.0020 g; [4-NP] = 35 μM; [$NaBH_4$] = 0.01 M; temperature = 25 °C. (d) Bar graph showing the effect of amount of Ca dopant on rate constant for the reduction of 4-NP.

the reactant has to be adsorbed onto the catalyst surface prior to reaction.

3.2.2. Effect of amount of dopant on catalytic activity

We also investigated the effect of the dopant dosage on catalytic activity by using Ca/Co_3O_4 catalyst since the Ca-doped catalyst was the most active catalyst in the reduction of 4-NP. The results obtained are plotted in Fig. 5(a) and the calculated apparent constants are shown in Fig. 5(b). The trend observed was that increasing the dosage from 1.1% to 2.4% increased the catalytic activity, while a further increase up to ~7% resulted in a decrease in activity. An explanation for this observation could be that at low (1.1% Ca) dosage there is not enough dopant hence low activity while high (7.0% Ca) dosages result in changes in both the morphology and change in the electronic structure of the Co_3O_4 as observed from the changes in H_2 consumption determined from H_2-TPR analysis (Fig. 3b). Therefore, 2.4% was used as an optimum doping dosage.

3.2.3. Langmuir–Hinshelwood kinetics

In order to study the kinetics of the reaction, we chose four different Ca doped catalysts, the optimum 2.4% Ca, the second most active 1.1% Ca, the middle 4.5% Ca and the least active 7.0% Ca. We ran several kinetic runs and determined the apparent rate constants, k_{app} from the absorption of 4-nitrophenol at λ 400 nm using Kinetic Studio Software. The obtained k_{app} values can be related to the rate at the surface, k and to the surface area, S of the catalysts through the Langmuir–Hinshelwood (L–H) Eq. (2).

$$k_{app} = \frac{k \cdot S \cdot K_{4NP}^{n}[4NP]^{n-1}(K_{BH_4^-}[BH_4^-])^{m}}{\{1 + (K_{4NP}[4NP])^{n} + (K_{BH_4^-}(BH_4^-)^{m}\}^{2}} \quad (2)$$

The other parameters in Eq. (2), K_{4NP} and $K_{BH_4^-}$ are the adsorption constants of 4-NP and borohydride respectively, n and m are the Freundlich exponents which describe the heterogeneity of the catalyst surface. The derivation of Eq. (2) is given in the Electronic Supplementary Information. From the Langmuir–Hinshelwood Eq. (2), the experimentally determined rate constants, k_{app}, were used to determine the surface rate constant, k, the Freundlich exponents, n and m as well as the adsorption constants for both 4-NP and borohydride, K_{4NP} and $K_{BH_4^-}$ using non-linear curve fitting. The plots of the k_{app} values versus [4-NP] and [$NaBH_4$] for the four catalysts studied are shown in Fig. 6(a) and (b) respectively. The solid lines in the two figures show the non-linear fitting curves obtained using Eq. (2). The parameters obtained from the fittings are summarized in Table 2 along with literature values obtained for heterogeneous catalyzed reductions of 4-NP.

From Fig. 6(a), increasing the concentration of 4-NP with a constant catalyst and borohydride concentration resulted in a decrease in the apparent rate constants. In contrast, an increase in the concentration of borohydride while keeping [4-NP] constant resulted in an initial increase in the apparent rate constants with a subsequent leveling off indicating that there is competition between 4-NP and $NaBH_4$ for the adsorption onto the catalyst surface as postulated by the Langmuir–Hinshelwood mechanism. This can be explained from the adsorption constants (K_{4NP} and $K_{BH_4^-}$) shown in Table 2, where adsorption of 4-NP is significantly larger than that of borohydride, with the consequence that at high [4-NP] most of the catalyst surface is occupied by 4-NP leaving less surface accessible to the borohydride and, therefore, the observed decrease in the apparent rate constants. On the other hand keeping [4-NP] constant while increasing borohydride concentration means initially the borohydride has more sites to adsorb onto and react with 4-NP but as the concentration increases these sites get saturated and any further increase in borohydride concentration results in a leveling off as seen in Fig. 6(b).

The L–H parameters obtained for the alkali and alkaline-earth doped Co_3O_4 catalysts were compared with the previously obtained parameters for undoped Co_3O_4 [29] and are shown in Table 2. The surface rate constants obtained for the doped catalysts were one order of magnitude larger than the undoped, with 2.4% Ca/Co_3O_4 having a value of $k = 8.47 \times 10^{-5}$ mol m^{-2} s^{-1} as compared to 5.33×10^{-6} mol m^{-2} s^{-1} for the undoped Co_3O_4 (Table 2). Also observed was that upon doping the adsorption constants for both 4-NP (K_{4NP}) and borohydride ($K_{BH_4^-}$) were higher than for the undoped Co_3O_4, an observation that may explain the enhanced catalytic activity. We also compared the L–H parameters obtained for our catalysts with those obtained for noble metals (Pt, Pd and Au) supported heterogeneous catalysts used in the reduction of 4-NP. From Table 2 doping the Co_3O_4 catalysts with Ca greatly improved the catalytic activity with surface rate constants getting closer to those of the supported noble metals, with 2.4% Ca/Co_3O_4 having a value of $k = 8.47 \times 10^{-5}$ mol m^{-2} s^{-1} and supported Pt, Au and Pd

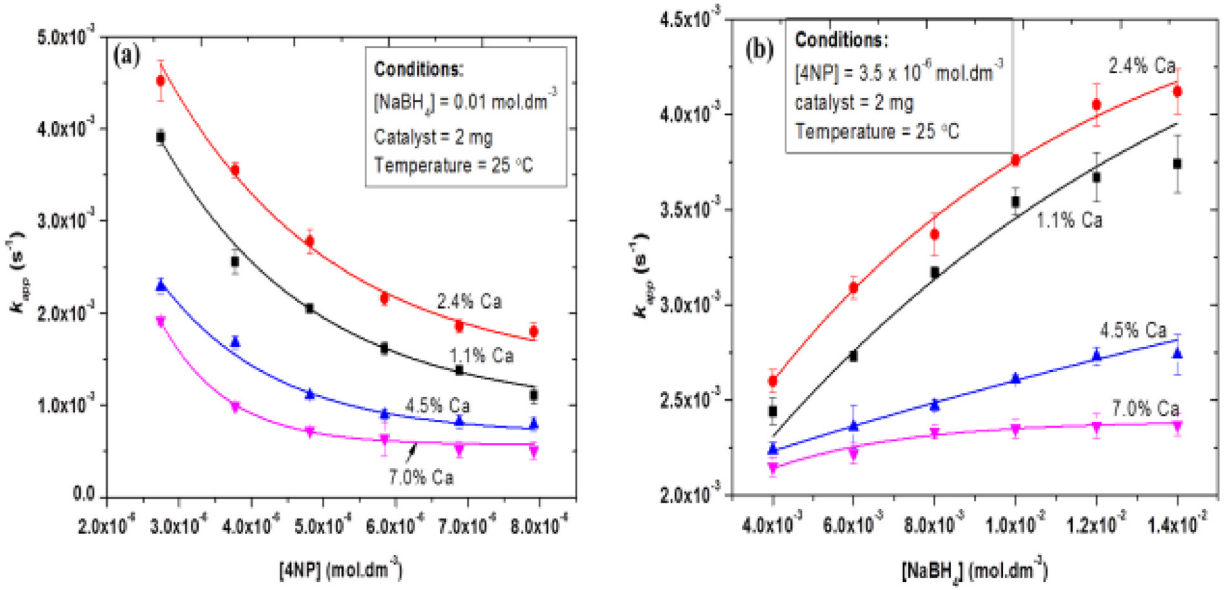

Fig. 6. Apparent rate constants as a function of (a) the concentration of 4-NP ([$NaBH_4$] = 0.01 M) and (b) the concentration of $NaBH_4$ ([4-NP] = 35 μM). Catalyst amount (2 mg) and temperature (25 °C) were kept constant in both variations. Data points show the experimental k_{app} values while solid lines are the L–H fitting curves.

Table 2
Parameters obtained from the fitting of the kinetic data to the L-H equation as well as values from other heterogeneous catalyzed reduction of 4-NP.

Catalyst	k (mol m^{-2} s^{-1})	K_{4NP} (L mol^{-1})	$K_{BH_4^-}$ (L mol^{-1})	n	m	References
1.1% Ca/Co_3O_4	5.85×10^{-5}	1005 ± 60	55 ± 8	0.80 ± 0.1	1.0 ± 0.2	This work
2.4% Ca/Co_3O_4	5.47×10^{-5}	1095 ± 55	58 ± 10	0.82 ± 0.05	1.0 ± 0.2	
4.5% Ca/Co_3O_4	3.25×10^{-5}	954 ± 30	40 ± 5	0.85 ± 0.2	1.0 ± 0.2	
7.0% Ca/Co_3O_4	9.80×10^{-6}	930 ± 75	50 ± 6	0.86 ± 0.2	1.0 ± 0.2	
undoped-Co_3O_4	5.33×10^{-6}	922 ± 40	22 ± 4	0.78 ± 0.2	1.0	Mogudi et. al. [29]
SPB-Pt	$(4.6 \pm 0.6) \times 10^{-4}$	2300 ± 500	89 ± 5	0.6 ± 0.1	0.78 ± 0.2	Wunder et al. [31]
SPB-Au	$(1.89 \pm 0.28) \times 10^{-4}$	5900 ± 900	76 ± 11	0.6 ± 0.1	1.0 ± 0.1	Wunder et al. [32]
SPB-Pd	$(5.5 \pm 0.5) \times 10^{-4}$	2300 ± 400	48 ± 5	0.6 ± 0.1	1.0 ± 0.1	Kaiser et al. [33]
Pd_{55}-DENs	$(1.09 \pm 0.25) \times 10^{-6}$	2569 ± 180	45 ± 9	0.43 ± 0.1	0.28 ± 0.1	Bingwa et al. [44]

SPB = spherical polyelectrolyte brushes.
DENs = dendrimer-encapsulated nanoparticles.

having values 4.6×10^{-4}, 1.89×10^{-4} and 5.5×10^{-4} mol m^{-2} s^{-1}, respectively.

3.3. Effect of varying temperature: determination of activation parameters

In order to determine the activation parameters (E_A, $\Delta H^{\#}$, $\Delta S^{\#}$ and $\Delta G^{\#}$) for the catalytic reduction of 4-nitrophenol (4-NP) we carried out the reaction at four different temperatures (20–35 °C) and obtained the apparent rate constants at each temperature as before. From the obtained apparent rate constants, we then calculated the activation energy (E_A) using the Arrhenius Eq. (3).

$$\ln\left(k_{app}\right) = \ln A - \frac{E_A}{RT} \tag{3}$$

The activation parameters, activation enthalpy ($\Delta H^{\#}$) and activation entropy ($\Delta S^{\#}$) were calculated using the Eyring Eq. (4).

$$ln\left(\frac{k_{app}}{T}\right) = -\frac{\Delta H^{\#}}{RT} + ln\left(\frac{k_B}{h}\right) + \frac{\Delta S^{\#}}{R} \tag{4}$$

From the values obtained for $\Delta H^{\#}$ and $\Delta S^{\#}$ we then calculated the Gibbs free-energy of activation $\Delta G^{\#}$. The Arrhenius and Eyring plots used to determine values for $\Delta H^{\#}$ and $\Delta S^{\#}$ are shown in the Supplementary information and all the activation parameters are summarised in Table 3.

The activation energy for the optimum 2.4% Ca loaded Co_3O_4 was the lowest of all the catalysts corresponding well to the highest catalytic activity observed experimentally. On comparison with the activation energies of colloidal metallic nanoparticles, which would be expected to have significantly lower E_A values and higher activities, our catalysts compared fairly well, with the 2.4% Ca/Co_3O_4 (E_A = 50.7 kJ mol^{-1}) having an E_A value only slightly higher than Pd supported on alumina (E_A = 43.0 kJ mol^{-1}) [45], Pd supported on spherical polyelectrolyte brushes (SPB) (E_A = 44.0 kJ mol^{-1}) [46] and Pt supported on Co and zeolite catalysts [47] (Table 3). The activation enthalpy value was positive and the activation entropy was negative, indicating that the reaction is endothermic and therefore energetically not favoured. The calculated $\Delta G^{\#}_{298}$ value was however, positive showing that the reaction is feasible in the presence of our catalysts as observed experimentally.

3.4. Reusability of the catalysts

To investigate the reusability of the cobalt oxide catalyst, we repeated the reduction of 4-NP with 2.4% doped Ca/Co_3O_4 catalyst in four cycles and calculated the apparent rate constants for each cycle. The rate constants remained relatively unchanged even after the fourth cycle as shown in Fig. 7(a). The mesoporous nanostructure of the catalyst remained unaltered as seen in the TEM image (Fig. 7b) showing the stability of the catalyst. Furthermore, ICP measurements showed no significant amount of cobalt in the

Table 3
Activation parameters for the reduction of 4-NP over *meso*-Co-X catalysts and a comparison with other similar systems reported in the literature.

Catalyst	E_A (kJ mol^{-1})	$\Delta H^{\#}$ (kJ mol^{-1})	$\Delta S^{\#}$ (J mol^{-1} K^{-1})	$\Delta G^{\#}_{298}$ (kJ mol^{-1})	References
2.4% Ca/Co_3O_4	50.7	53.2	−122	89.7	This work
Undoped Co_3O_4	51.3	97.4	63.1	78.6	Mogudi et al. [29]
Pd/Al_2O_3	43.0	–	–	–	Arora et al. [45]
SPB-Pd	44.0	–	–	–	Mei et al. [46]
CoY	60.0	–	–	–	El-Bahy [47]
Pt/CoY	55.0	–	–	–	
p(AMPS)-Co	27.8	–	–	–	Sahiner et al. [24]

Y = zeolite Y (faujasite); p(AMPS) = poly(2-acrylamido-2-methyl-1-propanesulfonic acid).

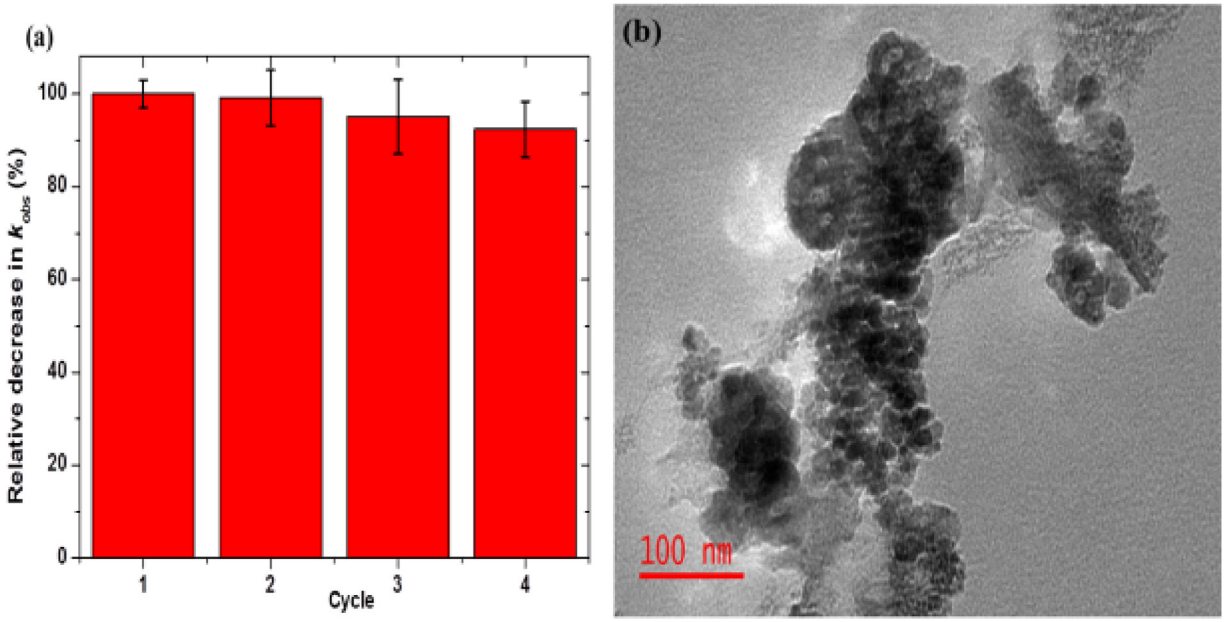

Fig. 7. (a) Graph showing the relatively unchanged k_{app} values for four cycles using 2.4% Ca/Co_3O_4 catalyst and (b) TEM image of 2.4% Ca/Co_3O_4 after the fourth cycle showing no significant change in the mesoporous structure of the catalyst.

supernatant after each run, indicating that no leaching of the catalyst into the aqueous media occurs. These results showed that the metal ion doped cobalt oxide catalysts prepared are stable and can be recycled and reused in the catalytic reduction of 4-NP.

4. Conclusions

We synthesized alkali and alkaline earth metal-doped Co_3O_4 catalysts and investigated the effect of doping on the catalytic activity on the reduction of 4-NP as a model reaction. From characterization techniques; XRD, SEM, TEM and BET, there were no significant structural changes upon doping the Co_3O_4 with Li, K, Cs, Mg and Ca. However, there was evidence of changes in the electronic structure of the Co_3O_4 catalysts upon doping from H_2-TPR analysis. The catalytic activity of the doped Co_3O_4 catalysts increased in the order Na < K < Li < Mg < Cs < Ca. The most active Ca doped Co_3O_4 were used to demonstrate that the reduction of 4-NP follows a Langmuir–Hinshelwood mechanism in a similar fashion as the undoped Co_3O_4. Langmuir–Hinshelwood parameters obtained for a 2.4% Ca/Co_3O_4; $k = 8.47 \times 10^{-5}$ mol m^{-2} s^{-1}, $K_{4NP} = 1095 \pm 60$ l mol^{-1} and $K_{BH_4^-} = 58 \pm 10$ l mol^{-1} were higher than those of the undoped Co_3O_4 with values of $k = 5.33 \times 10^{-6}$ mol m^{-2} s^{-1}, $K_{4NP} = 922 \pm 40$ l mol^{-1} and $K_{BH_4^-} = 22 \pm 4$ l mol^{-1}. The enhanced catalytic activity of the doped Co_3O_4 catalysts may have implications into replacing the more expensive noble metals in reduction reactions in synthetic chemistry.

Competing financial interest

The authors declare no competing financial interest.

Acknowledgements

We sincerely thank the National Research Foundation (NRF, South Africa) for funding through the research grant number 85386. We also thank the University of Johannesburg as well as Shimadzu (South Africa) for the instrumentation used.

Appendix A. Supplementary data

Supplementary data associated with this article can be found, in the online version, at http://dx.doi.org/10.1016/j.apcatb.2017.06.045.

References

[1] P. Yang, D. Zhao, D.I. Margolese, B.F. Chmelka, G.D. Stucky, Generalized syntheses of large-pore mesoporous metal oxides with semicrystalline frameworks, Nature 396 (1998) 152–155.
[2] Y. Ren, Z. Ma, P.G. Bruce, Ordered mesoporous metal oxides: synthesis and applications, Chem. Soc. Rev. 41 (2012) 4909–4927.
[3] C.T. Kresge, M.E. Leonowicz, W.J. Roth, J.C. Vartuli, J.S. Beck, Ordered mesoporous molecular sieves synthesized by a liquid-crystal template mechanism, Nature 359 (1992) 710–712.
[4] D. Zhao, J. Feng, Q. Huo, N. Melosh, G.H. Fredrickson, B.F. Chmelka, G.D. Stucky, Triblock copolymer syntheses of mesoporous silica with periodic 50–300 angstrom pores, Science 279 (1998) 548–552.

[5] A. Taguchi, F. Schüth, Ordered mesoporous materials in catalysis, Microporous Mesoporous Mater. 77 (2005) 1–45.
[6] Y. Wan, D. Zhao, On the controllable soft-templating approach to mesoporous silicates, Chem. Rev. 107 (2007) 2821–2860.
[7] C.-I. Ahn, H.M. Koo, J.M. Jo, H.-S. Roh, J.-B. Lee, Y.-J. Lee, E.J. Jang, J.W. Bae, Stabilized ordered-mesoporous Co_3O_4 structures using Al pillar for the superior CO hydrogenation activity to hydrocarbons, Appl. Catal. B: Environ. 180 (2016) 139–149.
[8] J. Gonzalez-Prior, J.I. Gutierrez-Ortiz, R. Lopez-Fonseca, G. Busca, E. Finocchio, B. de Rivas, Oxidation of chlorinated alkanes over Co_3O_4/SBA-15 catalysts. Structural characterization and reaction mechanism, Catal. Sci. Technol. 6 (2016) 5618–5630.
[9] S. Biswas, A.S. Poyraz, Y. Meng, C.-H. Kuo, C. Guild, H. Tripp, S.L. Suib, Ion induced promotion of activity enhancement of mesoporous manganese oxides for aerobic oxidation reactions, Appl. Catal. B: Environ. 165 (2015) 731–741.
[10] V.P. Santos, M.F.R. Pereira, J.J.M. Órfão, J.L. Figueiredo, Catalytic oxidation of ethyl acetate over a cesium modified cryptomelane catalyst, Appl. Catal. B: Environ. 88 (2009) 550–556.
[11] T. Grewe, H. Tuysuz, Alkali metals incorporated ordered mesoporous tantalum oxide with enhanced photocatalytic activity for water splitting, J. Mater. Chem. A 4 (2016) 3007–3017.
[12] A. Smuszkiewicz, J. Lopez-Sanz, I. Sobczak, M. Ziolek, R.M. Martín-Aranda, E. Soriano, E. Pérez-Mayoral, Mesoporous niobiosilicate NbMCF modified with alkali metals in the synthesis of chromene derivatives, Catal. Today 277 (2016) 133–142.
[13] L. Xue, H. He, C. Liu, C. Zhang, B. Zhang, Promotion effects and mechanism of alkali metals and alkaline earth metals on cobalt–cerium composite oxide catalysts for N_2O decomposition, Environ. Sci. Technol. 43 (2009) 890–895.
[14] M. Haneda, Y. Kintaichi, N. Bion, H. Hamada, Alkali metal-doped cobalt oxide catalysts for NO decomposition, Appl. Catal. B: Environ. 46 (2003) 473–482.
[15] M. Haneda, Y. Kintaichi, H. Hamada, Reaction mechanism of NO decomposition over alkali metal-doped cobalt oxide catalysts, Appl. Catal. B: Environ. 55 (2005) 169–175.
[16] N. Pasha, N. Lingaiah, N.S. Babu, P.S.S. Reddy, P.S. Prasad, Studies on cesium doped cobalt oxide catalysts for direct N_2O decomposition in the presence of oxygen and steam, Catal. Commun. 10 (2008) 132–136.
[17] T. Komatsu, T. Amaya, K. Otsuka, LiCl doped cobalt oxide is an active catalyst for the formation of ethylene in the oxidative coupling of methane, Catal. Lett. 3 (1989) 317–322.
[18] R. Patel, Promoting effect of transition metal-doped Co–B alloy catalysts for hydrogen production by hydrolysis of alkaline $NaBH_4$ solution, J. Catal. 271 (2010) 315–324.
[19] J. Haber, T. Machej, J. Janas, M. Nattich, Catalytic decomposition of N_2O, Catal. Today 90 (2004) 15–19.
[20] M. Konsolakis, I.V. Yentekakis, The reduction of NO by propene over Ba-Promoted Pt/γ-Al_2O_3 catalysts, J. Catal. 198 (2001) 142–150.
[21] M. Konsolakis, I.V. Yentekakis, Strong promotional effects of Li, K Rb and Cs on the Pt-catalysed reduction of NO by propene, Appl. Catal. B: Environ. 29 (2001) 103–113.
[22] I.V. Yentekakis, V. Tellou, G. Botzolaki, I.A. Rapakousios, A comparative study of the $C_3H_6 + NO + O_2$, $C_3H_6 + O_2$ and $NO + O_2$ reactions in excess oxygen over Na-modified Pt/γ-Al_2O_3 catalysts, Appl. Catal. B: Environ. 56 (2005) 229–239.
[23] A.M. Tafesh, J. Weiguny, A review of the selective catalytic reduction of aromatic nitro compounds into aromatic amines, isocyanates, carbamates, and ureas using CO, Chem. Rev. 96 (1996) 2035–2052.
[24] N. Sahiner, H. Ozay, O. Ozay, N. Aktas, A soft hydrogel reactor for cobalt nanoparticle preparation and use in the reduction of nitrophenols, Appl. Catal. B: Environ. 101 (2010) 137–143.
[25] H. Li, L. Han, J. Cooper-White, I. Kim, Palladium nanoparticles decorated carbon nanotubes: facile synthesis and their applications as highly efficient catalysts for the reduction of 4-nitrophenol, Green Chem. 14 (2012) 586–591.
[26] S. Saha, A. Pal, S. Kundu, S. Basu, T. Pal, Photochemical green synthesis of calcium-alginate-stabilized Ag and Au nanoparticles and their catalytic application to 4-nitrophenol reduction, Langmuir 26 (2010) 2885–2893.
[27] S. Harish, J. Mathiyarasu, K.L.N. Phani, V. Yegnaraman, Synthesis of conducting polymer supported Pd nanoparticles in aqueous medium and catalytic activity towards 4-nitrophenol reduction, Catal. Lett. 128 (2008) 197–202.
[28] K. Esumi, R. Nakamura, A. Suzuki, K. Torigoe, Preparation of platinum nanoparticles in ethyl acetate in the presence of poly(amidoamine) dendrimers with a methyl ester terminal group, Langmuir 16 (2000) 7842–7846.
[29] B.M. Mogudi, P. Ncube, R. Meijboom, Catalytic activity of mesoporous cobalt oxides with controlled porosity and crystallite sizes: evaluation using the reduction of 4-nitrophenol, Appl. Catal. B: Environ. 198 (2016) 74–82.
[30] T.R. Mandlimath, B. Gopal, Catalytic activity of first row transition metal oxides in the conversion of p-nitrophenol to *p*-aminophenol, J. Mol. Catal. A: Chem. 350 (2011) 9–15.
[31] S. Wunder, F. Polzer, Y. Lu, Y. Mei, M. Ballauff, Kinetic analysis of catalytic reduction of 4-nitrophenol by metallic nanoparticles immobilized in spherical polyelectrolyte brushes, J. Phys. Chem. C 114 (2010) 8814–8820.
[32] S. Wunder, Y. Lu, M. Albrecht, M. Ballauff, Catalytic activity of faceted gold nanoparticles studied by a model reaction: evidence for substrate-induced surface restructuring, ACS Catal. 1 (2011) 908–916.
[33] J. Kaiser, L. Leppert, H. Welz, F. Polzer, S. Wunder, N. Wanderka, M. Albrecht, T. Lunkenbein, J. Breu, S. Kummel, Y. Lu, M. Ballauff, Catalytic activity of nanoalloys from gold and palladium, Phys. Chem. Chem. Phys. 14 (2012) 6487–6495.
[34] A.S. Poyraz, W.A. Hines, C.-H. Kuo, N. Li, D.M. Perry, S.L. Suib, Mesoporous Co_3O_4 nanostructured material synthesized by one-step soft-templating: a magnetic study, J. Appl. Phys. 115 (2014).
[35] Kinetic Studio, TgK Scientific Limited, Bradford-on-Avon, 2010, pp. Transient Kinetics and Spectroscopy software.
[36] OriginPro, OriginLab Corporation, Northampton, 2014, pp. Data Analysis and Graphing software.
[37] A.S. Poyraz, C.-H. Kuo, S. Biswas, C.K. King'ondu, S.L. Suib, A general approach to crystalline and monomodal pore size mesoporous materials, Nat. Commun. 4 (2013).
[38] W. Song, A.S. Poyraz, Y. Meng, Z. Ren, S.-Y. Chen, S.L. Suib, Mesoporous Co_3O_4 with controlled porosity: inverse micelle synthesis and high-performance catalytic CO oxidation at −60 °C, Chem. Mater. 26 (2014) 4629–4639.
[39] C.-B. Wang, C.-W. Tang, S.-J. Gau, S.-H. Chien, Effect of the surface area of cobaltic oxide on carbon monoxide oxidation, Catal. Lett. 101 (2005) 59–63.
[40] M. Kang, M.W. Song, C.H. Lee, Catalytic carbon monoxide oxidation over CoOx/CeO_2 composite catalysts, Appl. Catal. A: Gen. 251 (2003) 143–156.
[41] L.F. Liotta, G. Di Carlo, G. Pantaleo, A.M. Venezia, G. Deganello, Co_3O_4/CeO_2 composite oxides for methane emissions abatement: relationship between Co_3O_4–CeO_2 interaction and catalytic activity, Appl. Catal. B: Environ. 66 (2006) 217–227.
[42] L. Xue, C. Zhang, H. He, Y. Teraoka, Catalytic decomposition of N_2O over CeO_2 promoted Co_3O_4 spinel catalyst, Appl. Catal. B: Environ. 75 (2007) 167–174.
[43] G.S. Sewell, E. van Steen, C.T. O'Connor, Use of TPR/TPO for characterization of supported cobalt catalysts, Catal. Lett. 37 (1996) 255–260.
[44] N. Bingwa, R. Meijboom, Kinetic evaluation of dendrimer-encapsulated palladium nanoparticles in the 4-nitrophenol reduction reaction, J. Phys. Chem. C 118 (2014) 19849–19858.
[45] S. Arora, P. Kapoor, M.L. Singla, Catalytic studies of palladium nanoparticles immobilized on alumina synthesized by a simple physical precipitation method, React. Kinet. Mechan. Catal. 99 (2010) 157–165.
[46] Y. Mei, Y. Lu, F. Polzer, M. Ballauff, M. Drechsler, Catalytic activity of palladium nanoparticles encapsulated in spherical polyelectrolyte brushes and core-Shell microgels, Chem. Mater. 19 (2007) 1062–1069.
[47] Z.M. El-Bahy, Preparation and characterization of Pt-promoted NiY and CoY catalysts employed for 4-nitrophenol reduction, Appl. Catal. A: Gen. 468 (2013) 175–183.